LASER INTERFEROMETER GRAVITATIONAL WAVE OBSERVATORY
-LIGO-
CALIFORNIA INSTITUTE OF TECHNOLOGY
MASSACHUSETTS INSTITUTE OF TECHNOLOGY

Technical Note **LIGO-T040066- 00- E** 04/13/2004

The Effect of Thermal Lensing on Wave-Front Sensor signals

Biplab Bhawal

This is an internal working note
of the LIGO Project.

California Institute of Technology
LIGO Project - MS 18-34
Pasadena CA 91125
Phone (626) 395-2129
Fax (626) 304-9834
E-mail: info@ligo.caltech.edu

Massachusetts Institute of Technology
LIGO Project - MS NW17-161
Cambridge, MA 02139
Phone (617) 253-4824
Fax (617) 253-4824
E-mail: info@ligo.mit.edu

WWW: http://www.ligo.caltech.edu/

file /home/malik/docs/ps/T040066.ps

1 Introduction

Correct prediction of Wave front sensor signals is crucial for implementing a robust Alignment Sensing and Control (ASC) system for LIGO. Unfortunately, due to heating of the mirrors by high laser power and the consequent effect of thermal lensing, the situation becomes complicated. Thermal lensing mainly affects the sidebands in LIGO I and so with increasing power their overlap with carrier may change and this may lead to changes in wave front sensor signals from the time the light first enters into the interferometer to the final saturation point of heating.

The one-point design solution[1] for thermal lensing in LIGO I ensures perfect mode-matching of light in the final hot state. However, the as-built parameters differ from the designed value and the input power may also differ depending on various factors. This may prevent the interferometer to reach the designed "hottest" state.

The program of thermal compensation for nullifying the effect of thermal lensing started in January, 2004. If this attempt becomes successful, the problem of arriving at the best mode-matched state with any set of deviated parameter values from the designed ones would be easier. However, a proper understanding of the effects of heating on WFS would still be helpful for proper commissioning and operation of the interferometers.

In this note such changes are described in detail. A number of the trends described here were observed in Hanford 4km interferometer.

The main program we use for studying this problem is the MIT FFT code[2] which has been recently upgraded by Hiro Yamamoto at Caltech mainly to have better computational speed and to have additional port outputs like Pox, Poy, Pob which were not available in the original program and also to introduce a feature to set different refractive indices to different mirrors which, as explained in section 3, is needed for studying effects of differential heating.

Matlab tools have been written to take field outputs (in the form of 128 X 128 pixel grid) from FFT code as input, express those in Hermite-Gaussian basis upto order $m + n = 20$ (which was found to be good enough to calculate WFS signals with less than 1% accuracy) and propagate those to appropriate distances (in terms of Gouy phase) and then calculate WFS signals at split-photodetectors. Note that propagation this way (by multiplying each spatial mode by appropriate Gouy phase) could differ from the simulation of actual telescope which is meant to be giving an equivalent Guoy phase to the beam. In actual telescope the beam size is drastically reduced and thus its modal basis also changes quite a lot. However, we expect to establish correspondence of these simulation results with the relative sizes of signals, when properly measured avoiding other perturbations like rotation or shifting of the beam wrt the split photodetector.

Throughout this note, we express WFS signals using same normalization procedure as of the 1998 paper by Fritschel et al[3] that provided theoretical values of WFS signals for a 6-optics interferometer with parameters that were different from as-built LIGO. More about this is discussed in section 4.

2 Abbreviations used in this note

Frequencies:

- CR - carrier
- RRSB - Resonant (in recycling cavity) SideBand (frequency about 24 Mhz)
- NRSB - Non-Resonant Sideband (frequency about 61 Mhz)
- SBP - Positive sideband
- SBM - negative sideband

Mirrors and alignment degrees of freedom:

- ITM - Input Test Mass
- ITMX - ITM of X-arm
- ITMY - ITM of Y-arm
- ETM - End Test Mass
- DETM - Differential mode misalignment in ETMs
- DITM - Differential mode misalignment in ITMs
- CETM - Common mode misalignment in ETMs
- CITM - Common mode misalignment in ITMs
- RM - Recycling Mirror or its misalignment which is always in common mode.

Others:

- dof - degree of freedom
- IFO - interferometer
- H1 - LIGO Hanford 4 km IFO
- Pox - Pick off beam from AR side of ITMX
- Poy - Pick off beam from AR side of ITMY
- ROC - radius of curvature
- TEM - Transverse Electromagnetic modes
- WFS - Wave Front Sensor

3 Mimicking Thermal Lensing

The target sensitivity of LIGO requires the use of very high light power, 20 kWatt in arms, to reduce the photon shot noise. Absorption of a small fraction of this power in the optical components can lead to serious degradation of the performance of the interferometer.

The temperature gradient inside the substrate leads to the gradient of refractive index and thus optical path length across transverse direction. This leads to changes in transmitted beam wavefront and is called *Thermal lensing*[4].

In LIGO I the main contribution of this effect comes from input mirrors. So, even if the input light is prepared to be the fundamental eigenmodes of the cavities, due to thermal lensing the light may still be mode-mismatched and so not perfectly resonant in the cavity. Analytical calculation and some careful FFT modeling show that there is negligible effect of thermal lensing on carrier in LIGO 1st generation interferometer because the carrier modes are mainly determined by arms which are large compared to the recycling cavity.

However, the situation is different for sidebands which are coupled into only the recycling cavity and does not enter the arms. The recycling cavity length (about 9 meter) is much smaller than the radii of curvature (about 15 km) of the recycling mirror or the input mirrors constituting the cavity. Under such a situation, the cavity approaches a *degenerate* state which means it does not have any preferred eigenmode to select. This is serious situation because most of the higher order modes that may get created due to any kind of perturbation may get resonant in such a cavity and, with much of higher order modes, the cavity may become unstable.

Thermal lensing affects the mode-matching of the sidebands in a big way as it goes through the dielectric of the input mirrors, gets totally reflected from its surface and gets into the recycling cavity again. The amount of heat absorbed in Input mirror has two components:

$$\begin{aligned} \text{Substrate heat absorption} &= \text{Input Power} \times \text{Recycling Gain} \\ &\quad \times \text{Substrate absorption coefficient}, \qquad (1) \\ \text{Surface heat absorption} &= \text{Input Power} \times \text{Recycling Gain} \times \text{Arm Gain} \\ &\quad \times \text{Surface absorption coefficient}, \qquad (2) \end{aligned}$$

In LIGO I the input power entering the recycling mirror is about 6 Watt and recycling gain is about 50 and arm gain is about 133. So, the power in recycling cavity between the recycling mirror and beam-splitter is about 150 watt, while the arm power is about 20 kWatt. Note that in Eq.2 only the surface absorption from the arm side of the input mirror(s) is considered because its effect is much more than the absorption from the recycling cavity side. Any difference in these absorption coeffecients and reflectivities (which determine Gains) between optics in two arms causes difference in the level of mode-matching in two sides of the interferometer and may lead to more difficulties in its operation.

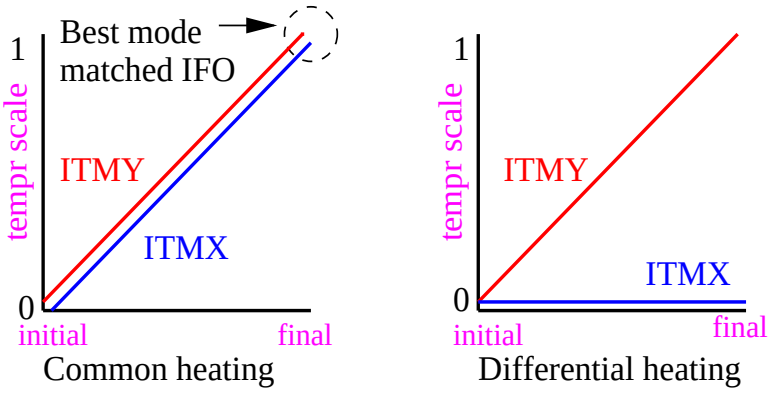

Figure 1: Common (left) heating and an extreme case of Differential heating. The heating is expressed in a scale of '0' (initial cold) to '1' (final hot) for each arm ITM. Note that LIGO I was designed such that at this 'theoretical' final hot state, the input beam would be best mode-matched.

In this note we mimick thermal lensing in LIGO I by effective changes in refractive indices of the ITMs. LIGO's one-point design solution for thermal lensing ensures best mode-matching in the hottest state achievable with the planned laser of 10 Watt power. For any deviation from that state (due to any difference between the designed and as-built parameters), the problem of thermal lensing is manifested by mode-mismatch that may happen especially to any sideband which enters through ITM dielectric and gets lensed to have an ROC value different from ITM ROC on the HR side from where the SB gets reflected back into the recycling cavity.

For LIGO Hanford 4 km interferometer the hottest state corresponds to ITM refractive index of about 0.96 and the cold state is nothing but the fused silica refractive index of 1.45. The value of 0.96 can be obtained by finding out best-matched modal parameters for average ROC values of corresponding mirrors in two arms of the as-built H1 interferometer.

In this note we describe these and any intermediate state in a scale of 0 (initial cold state) to 1 (the hottest state for the designed LIGO I). Whatever the laser power is, the IFO always starts in state 0 and slowly approaches state 1. Depending on available input power or some other known or undetected deviation from as-built LIGO, the IFO may or may not reach state 1 in its saturated state. Success in ongoing thermal compensation may solve this problem originating from such deviations.

In this note we refer to two different kinds of heating that may take place in IFO. As Fig.1 shows, these are (i) Common heating: in which case both arms get heated in the same way, and (ii) Differential heating: in which case arms may get heated in a dfifferent way. The figure shows an extreme case of differential heating in which only ITMY gets heated, while ITMX remains in cold state. We consider such an imaginary case in our discussion just for the sake

of bringing out features related to such heating in a prominent way, which may otherwise be suppressed under the effect of common heating. We can say that common heating would be more prominent than differential heating because, in case it were not so, too much different absorption coefficients in two arms would have led to serious reduction in Carrier gains - somthing which has not been observed in H1.

As already discussed, heating mainly affects SBs. Here is a rough idea of the field contents in various heated states: In a cold (0) state, about 63% of SB power remains in higher order modes, whereas for the hottest (1) state in both arms, this value is less than 1%. For the hottest state in the extreme cases of differential heating as illustrated above, about 42% (on average) SB power goes into higher order modes. Under such a condition difference in upper and lower SBs has been observed in simulation. Their power may differ by about 19% in the case of extreme differential heating considered.

4 Introduction to Wavefront Sensor Signals

The misalignment signals from 6 optics LIGO system have been systematically studied with Modal Model code developed in Mathematica at MIT for both static [3] and dynamic[5] cases. The static case results have also been validated against E2E model (developed at Caltech) [6] and the FFT code developed at MIT[2] and the details of this comparison have been recorded in a LIGO document[7].

For calculation of WFS signals in this note, we follow the same normalization procedure of the 1998 paper by Fritschel et al[3]

This contribution of various dofs in a particular WFS is given by Eq.(16) of Ref[3], describing the RF amplitude-modulated alignment signal at each port as:

$$WFS(\eta, \Theta, \Gamma) = P_{in} f(\Gamma) f_{split} k_{PD}^{10} \sum_{i=1}^{5} A_i \Theta_i \cos(\eta - \eta_i) \cos(\omega_m t - \phi_{Di}) \qquad (3)$$

where P_{in} is the total power, Γ is the modulation index, Θ_i, the normalized angles wrt the divergence angle. f_{split} and k_{PD}^{10} are less-than-unity factor accounting for the difference between the specific photodiode geometry and the idealized half-plane detector. $f(\Gamma) = 2J_0(\Gamma)J_1(\Gamma)$, where J is Bessel function.

Table 2 of the paper presents the numbers A_i representing normalized signal amplitude for each dof i and η_i representing the corresponding Gouy phase of propagation needed to maximize the signal. For details of these calculations see Ref.[3, 7].

The suitable Gouy phase ($\eta = \eta_i$) location for each WFS where the signal for the target dof i gets maximized can also be calculated analytically like this:

[We may note here that the WFS signal contributions (measured in split-photodetectors) come from two frequencies (like CR and SBP) with spatial modes TEM$_{mn}$ such that 'm' remains same (considering pitch mode only) for both frequencies and 'n' differ by some odd

number. It is found that main contribution always come from terms like CR00 and SB01. Under a cold condition, SBs contain lot of higher order modes originating from mode-mismatch, like 02, 04 etc. But their possible companion could be CR01, CR03 etc. Such combinations contributes much less than that of CR00 and SB01 etc]

The following 8 amplitudes represent the coefficients of the Hermite-Gaussian modes at any output port of the IFO: The Carrier TEM00, $\overline{\mathrm{CR}}_{00}$, the carrier TEM01 (for pitch modes), $\overline{\mathrm{CR}}_{01}$, the positive sideband TEM00, $\overline{\mathrm{SBP}}_{00}$, the positive sideband TEM01, $\overline{\mathrm{SBP}}_{01}$, the negative sideband TEM00, $\overline{\mathrm{SBM}}_{00}$, the negative sideband TEM01, $\overline{\mathrm{SBM}}_{01}$.

The *quadrature* and *in-phase* signals are then calculated as

$$Q = 2\mathrm{Re}\Big[S_1 e^{-i\eta} + S_2 e^{+i\eta} + S_3 e^{-i\eta} + S_4 e^{+i\eta}\Big] \quad (4)$$

$$I = -2\mathrm{Im}\Big[S_1 e^{-i\eta} + S_2 e^{+i\eta} + S_3 e^{-i\eta} + S_4 e^{+i\eta}\Big] \quad (5)$$

where

$$S_1 = \overline{\mathrm{CR}}_{00}\overline{\mathrm{SBP}}^*_{01} \quad (6)$$

$$S_2 = \overline{\mathrm{CR}}_{01}\overline{\mathrm{SBP}}^*_{00} \quad (7)$$

$$S_3 = \overline{\mathrm{SBM}}_{00}\overline{\mathrm{CR}}^*_{01} \quad (8)$$

$$S_4 = \overline{\mathrm{SBM}}_{01}\overline{\mathrm{CR}}^*_{00} \quad (9)$$

where * represents the conjugation and η is the Gouy phase between the TEM00 and TEM01 modes at the output ports. If R_i and I_i represent the real and imaginary parts respectively of S_i, then the signals with corresponding Gouy phases can be expressed as

$$Q = 2[(R_1 + R_2 + R_3 + R_4)^2 + (I_1 - I_2 + I_3 - I_4)^2]^{1/2} \quad (10)$$

$$\eta_Q = tan^{-1}\left[\frac{(I_1 - I_2 + I_3 - I_4)}{(R_1 + R_2 + R_3 + R_4)}\right] \quad (11)$$

$$I = -2[(I_1 + I_2 + I_3 + I_4)^2 + (R_2 - R_1 + R_4 - R_3)^2]^{1/2} \quad (12)$$

$$\eta_I = tan^{-1}\left[\frac{(R_2 - R_1 + R_4 - R_3)}{(I_1 + I_2 + I_3 + I_4)}\right] \quad (13)$$

As is illustrated in following sections, heating may alter the field amplitudes and phases of the Sidebands and their relative phases wrt the carrier, which may affect signal amplitudes, their Gouy phases and even the demodulation angle. The telescope for each WFS should be properly located and set to take care of these effects and to have good level of separation of various dofs.

5 Heating effects on WFS signals

The current (During Science runs S2 and S3) implementation of WFS system for H1 is as follows. The locations of the quadrant photodetectors for different WFSs with the corresponding

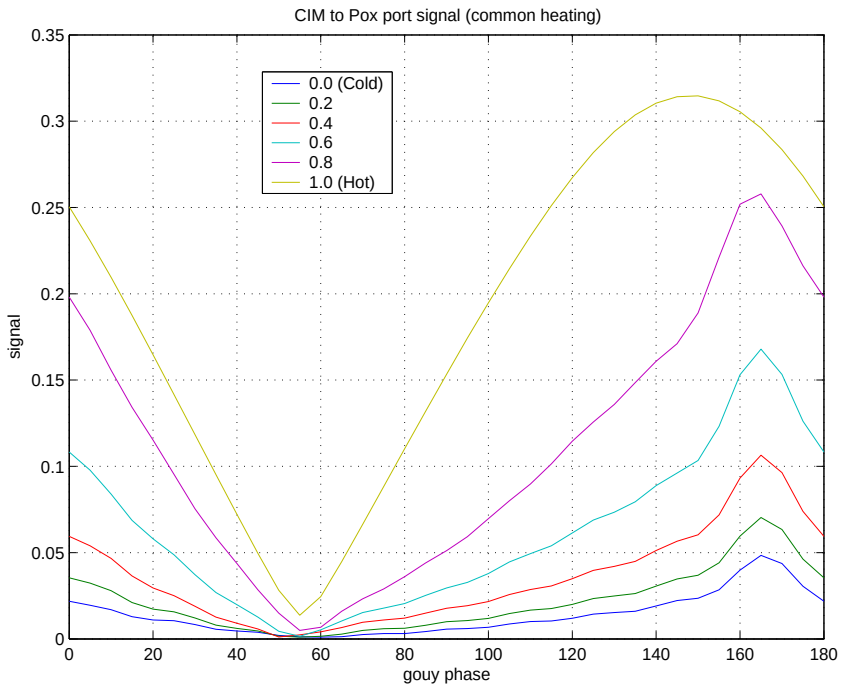

Figure 2: WFS2a inphase signal for CITM dof as function of Gouy phase from the port.

target dof that each wants to measure are like this:

- Dark port (RRSB demodulation): WFS1 (quadrature phase) –> DETM
- Pox port (RRSB demodulation): WFS2A (inphase) –> CITM, WFS2B (quadrature phase) –> DITM
- Reflected port (NRSB demodulation): WFS3 (inphase) –> CETM
- Reflected port (NRSB demodulation): WFS4 (quadrature phase) –> RM

In the following three subsections we discuss variation of these signals at the three ports where those are measured.

5.1 WFS signals: Pox port

WFS 2 measures the signals from the pick-off beam coming from the Pox port. The aim is to measure CITM and DITM signals at WFS2a and WFS2b in inphase and quadrature phase respectively. Both the carrier and sidebands generate higher order components due to

misalignments in ITMs. In any cold state the sidebands get quite a good amount of higher order modes. Figures 2 3 and show how these two types of signals get affected by heating.

The strategy followed at the site is to minimize the contribution of RM dof (which is a pure common alignment mode) in WFS2b signal and extract mainly the DITM contibution there.

Here we look into some details of these two types of signals: (i) Common mode of misalignment: RM dof (Note that CIM signal follows the same pattern as that of RM but they differ from RM signal by $\sqrt{2}$ in the normalization followed in Ref.[3]) and (ii) Differential misalignment: DITM dof. Fig.4 shows variation in demodulation angle by several degrees in all cases of differential heating but not much of that variation in common heating when only common alignment is perturbed. Common heating with DITM dof also shows changes in demodulation angle. Fig.5 shows differential heating cases for both common and differential misalignment dof.

Such variation of demodulation angle is found to be related to the variation of amplitudes and phases of SBP and SBM for which they rotate differently wrt the carrier. Fig.6 plots variation in SBP and SBM as function of differential heating of two types: either only ITMX or only ITMY is heated while the other remains cold.

Such variation of demodulation angle in WFS2 signals were observed in H1. According

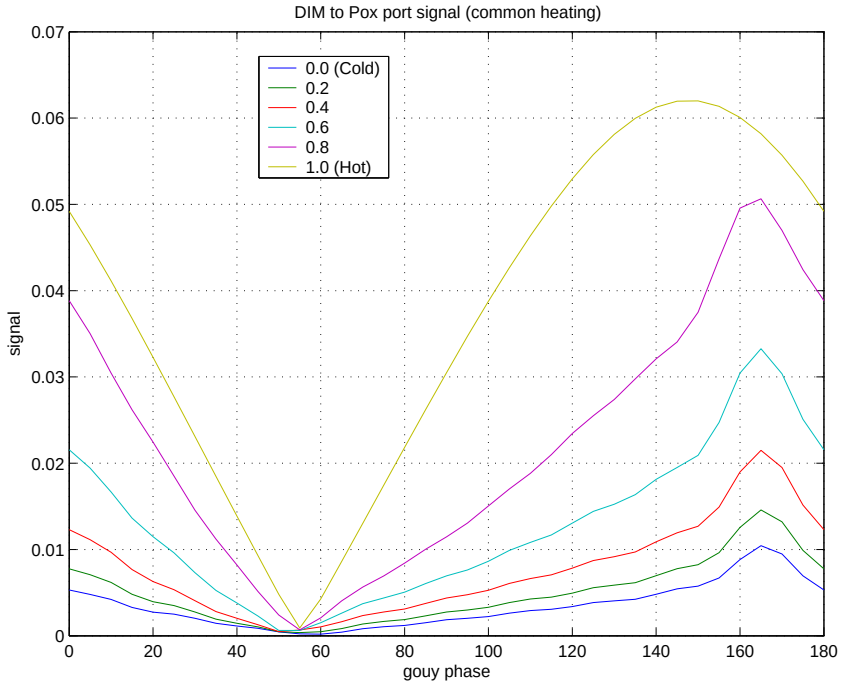

Figure 3: WFS2b quadrature phase signal as function of Gouy phase from the port.

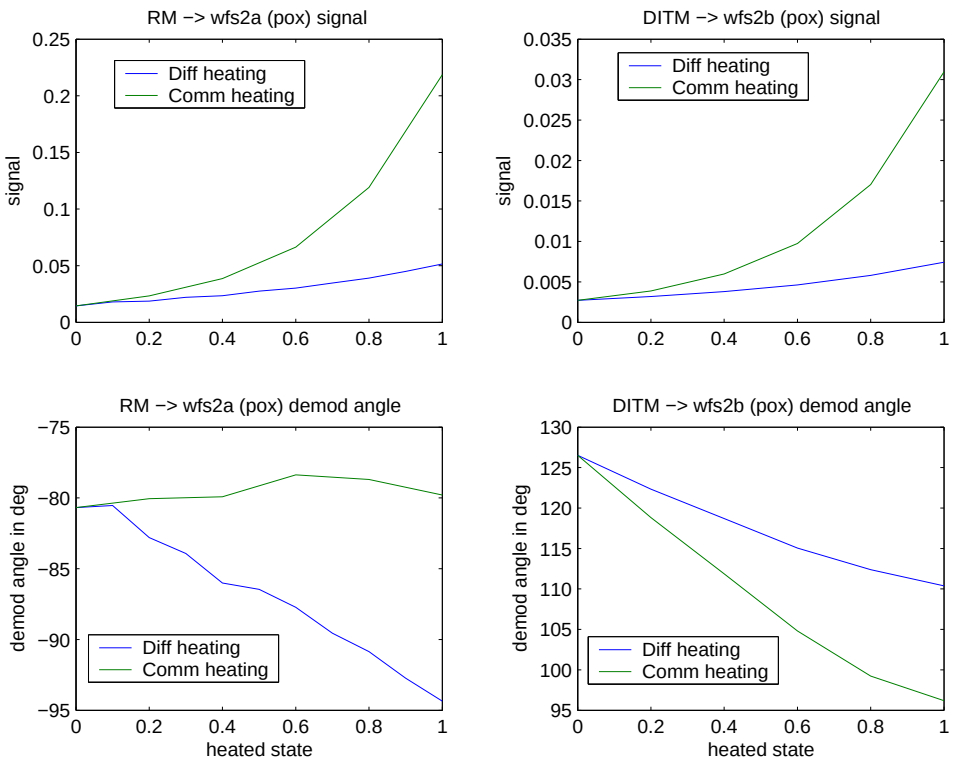

Figure 4: The changes in WFS2 signals and demodulation angles for common (RM) and differential (DITM) misalignment modes under various differentially heated states at Gouy phase value of 145 degree

to the latest measurement[9], the rotation of about 35 degree was recorded by increasing the input power to IFO from 800 mW to about 2.3 W. Considering extreme cases of differential heating in simulation we observed rotation by about 15 degrees in WFS2a signal for common mode and about 30 degrees in WFS2b for DITM dof. However, as already mentioned, if differential heating of this extent had taken place, that would have been manifested in other ways too, e.g. in carrier gain. However, variation of 30 degrees in common heating for DITM dof could possibly explain this effect. However, this value in simulation was obtained between initial cold and final hottest state, whereas the variation observed in H1 is between IFO states with input power of 800 mW and 2.3 W respectively, which do not cover the full range of heated states. More measurements and analysis would be necessary to make these number agree quantitatively.

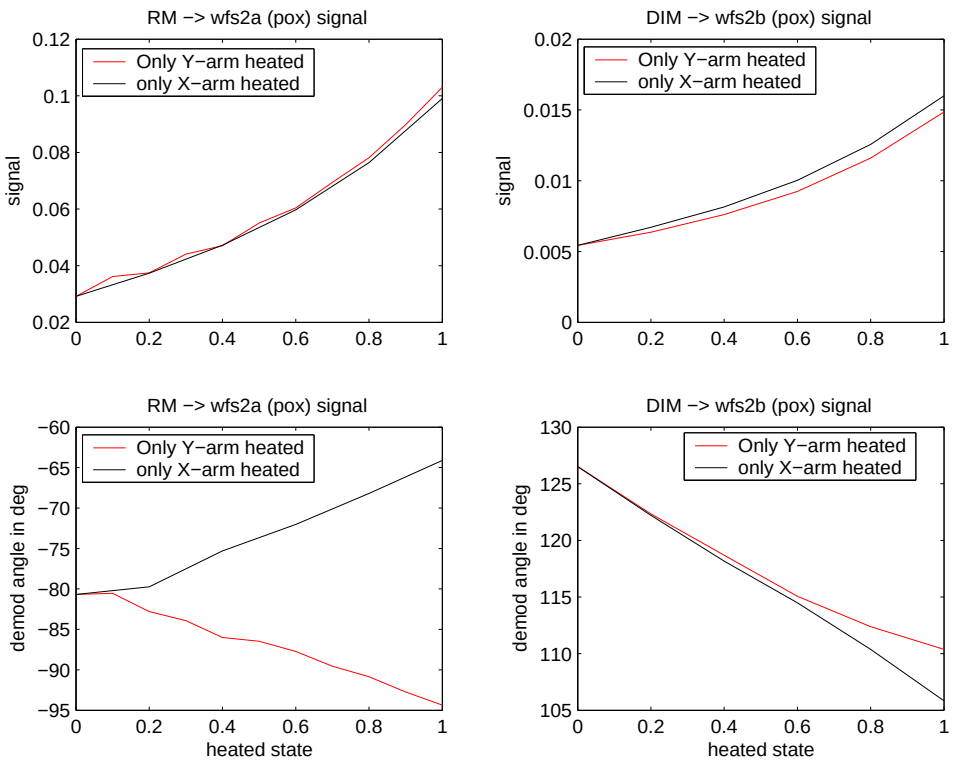

Figure 5: The changes in WFS2 signals and demodulation angles for common (RM) and differential (DITM) misalignment modes under various differentially heated states at Gouy phase value of 145 degree

.

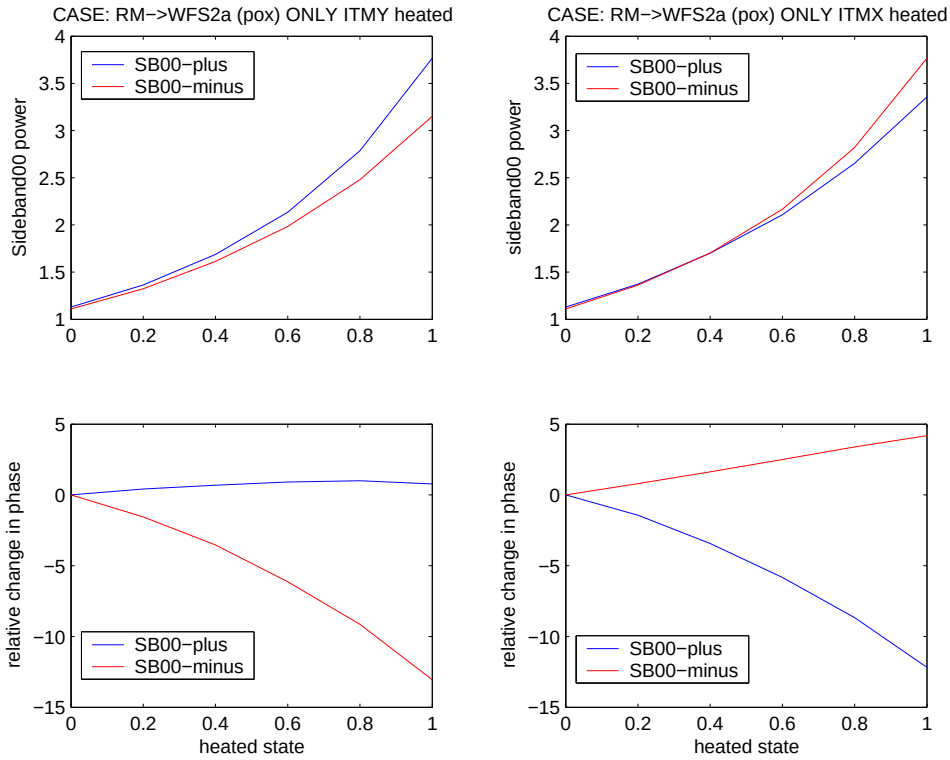

Figure 6: Changes in SB power and phase for two different types of differential heating: In one (left side) only Y-arm is heated. In the other case (right side) only X-arm is heated.

.

5.2 WFS signals: Reflected port

WFS 3 and 4 are placed at the reflected port. In this section we describe the contribution of various common mode effects on these two WFSs which are measured at demodulation frequency of the NRSB.

Since the modulation on LIGO laser is done in series: NRSB is modulated over both carrier and RRSBs. These sidebands on sidebands, ie., NRSB * SB, have strength which is proportional to $\Gamma_{\rm SB}\Gamma_{\rm NRSB}$. For WFS 3 and 4 at the reflected port, the main contribution in signals comes from 3 terms:

1. CR with upper and lower NRSB (proportional to $\Gamma_{\rm NRSB}$)
2. upper RRSB with (RRSB $\pm$ NRSB) (proportional to $\Gamma^2_{\rm RRSB}\Gamma_{\rm NRSB}$)
3. lower RRSB with ($-$ RRSB $\pm$ NRSB) (proportional to $\Gamma^2_{\rm RRSB}\Gamma_{\rm NRSB}$)

The last two terms are important because the alignment signals of the resonant SBs are amplified by the degeneracy of the recycling cavity and that $\Gamma^2_{\rm SB}$ isn't really small.

On the other hand, it may be noted that the thermal effect does not at all affect the contribution of the CETM dof in the reflected port WFS signal demodulated by NRSB. The effect of CETM is experienced by only the carrier which alone is resonant in the arms. As a result no contribution comes from terms 2 and 3 above. Since NRSB does not enter the interferometer it does not get affected by heating effect anyway. As we have already pointed out, at

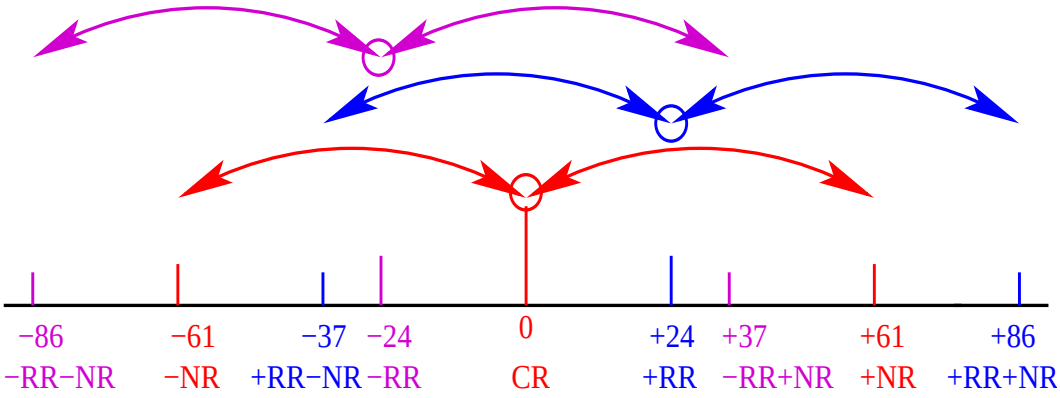

Figure 7: This figure represents 3 combinations of beams of different frequencies that may contribute to the WFS signals at the reflected port which are demodulated at the Non-Resonant (NR) sideband frequency of about 61 Mhz. 'CR' and 'RR' represent the reference carrier frequency and the resonant (in recycling cavity) upper sideband frequency of about 24 Mhz respectively

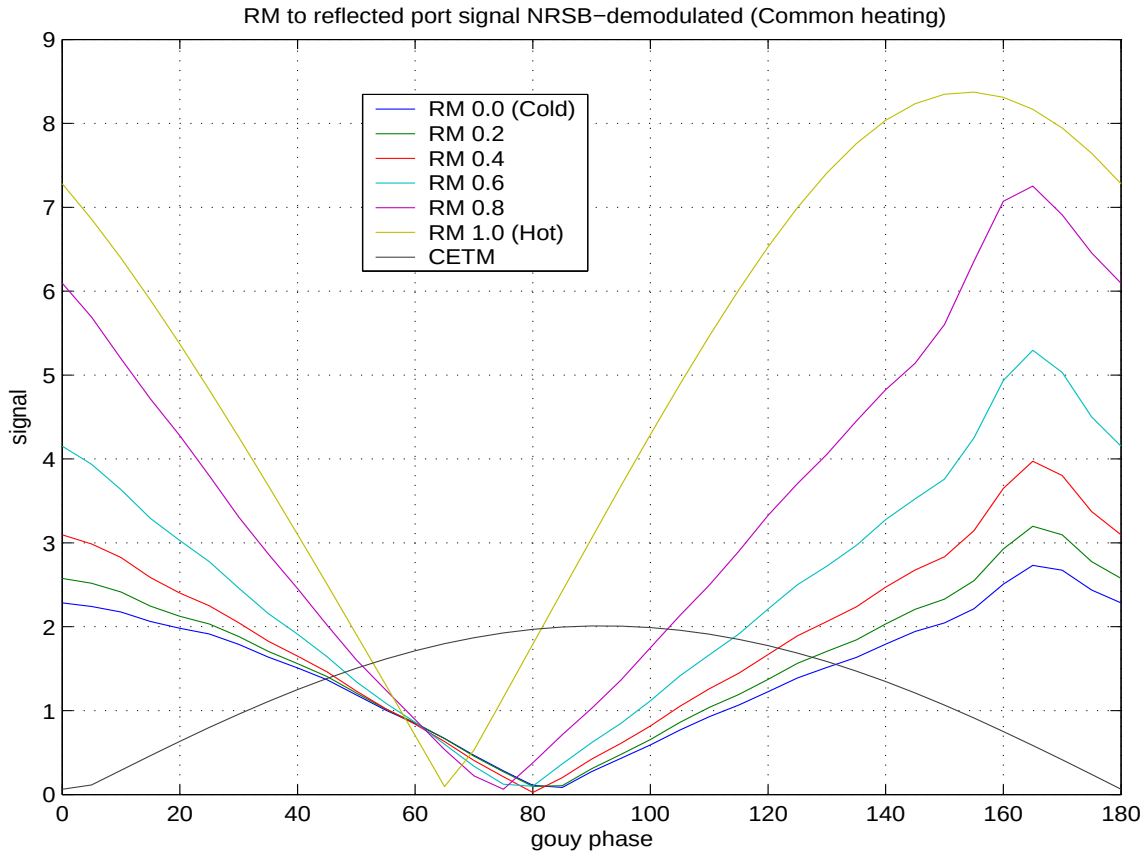

Figure 8: The WFS signal for RM dof under various heated conditions (in the scale of 0 for initial cold and 1 for final hot) at the reflected port as a function of Gouy phase from the port. The signal contribution from CETM dof is also shown. Note: CETM signal does not get affected by heating

least in LIGO I, the carrier, in any case, does not get affected by the heating effect and so the contribution from term 1 also remains independent of heating.

Figure8 shows the changes in the contribution of the RM dof under various heated condition and corresponding Gouy phases. The contribution of CETM dof is also plotted on it so that a good decision for the correct location of WFS 3 and 4 can be made. If WFS3 is to be set for measuring CETM dof, then the signal of RM should be minimized there. Note how the minimum Gouy phase point for RM dof move as a function of heating. In the cold state if the Gouy phase is set to 80-90 degrees, one may get well-separated maximized signal for CETM. However, with heating the RM signal increases there and the minimum point moves and the signals may get mixed up. The best value to set is about 60-65 degree where RM is always lower than CETM signal under any heated condition. The natural choice for WFS4 location

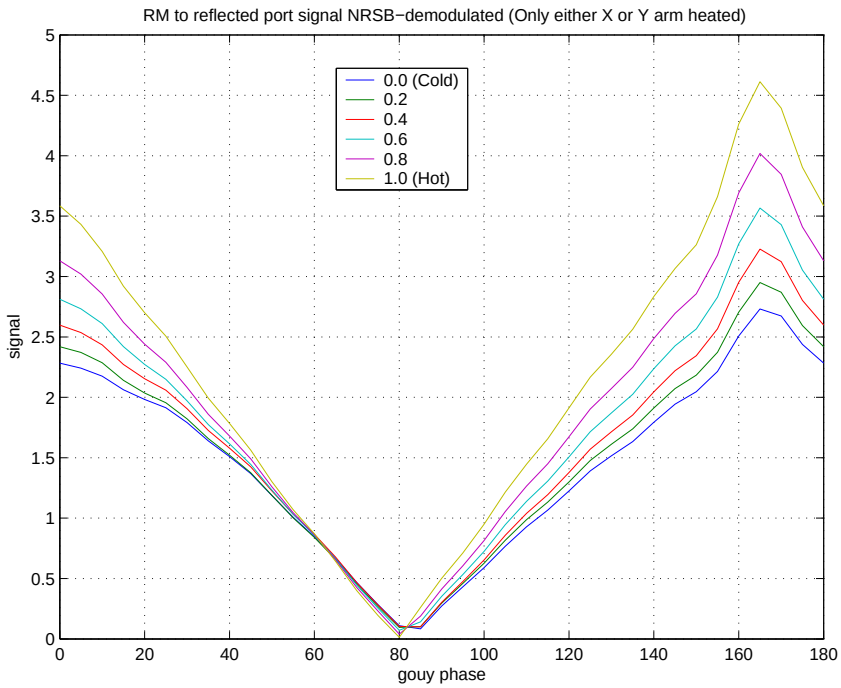

Figure 9: The WFS signal for RM dof under extreme differential heated conditions at the reflected port as a function of Gouy phase from the port.

would be 90 degree apart at about 150 degree where RM signal remains near its maximum point under any heated condition. However, differential heating may alter such considerations as shown in Fig.9 for extreme case of such heating.

As a check, note that the contribution of the remaining common mode signal, CITM, at either of the above locations for WFS3 or 4 remains low as compared to the contributions from CETM or RM respectively. The CITM contribution is shown in Fig10.

The measurements of best settings of telescopes at H1 conforms with this observation[8]. The WFS3 and WFS4 telescopes at H1 are currently set at 60 degree and 150 degrees respectively to get good separation of signals at both locations. The ratio of $\sim 1/10$ measured for CETM/RM and CITM/RM for WFS4 agrees with observation made in Fig.8 and 10.

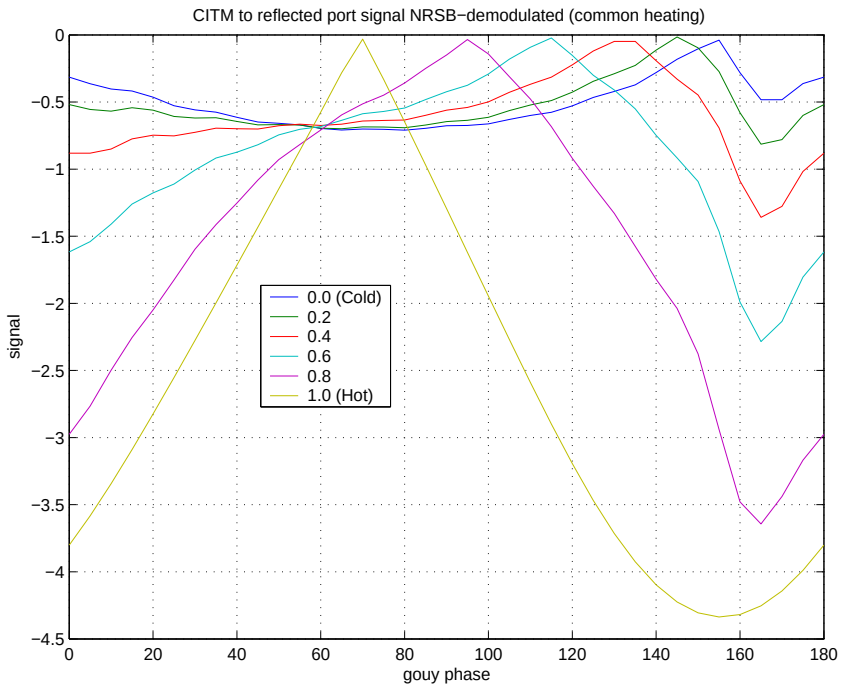

Figure 10: The WFS signal for CITM dof under various common heated conditions at the reflected port as a function of Gouy phase from the port.

5.3 WFS1 signal: Dark port

Fig.11 shows how the WFS1 signal for DETM dof varies with common heating. Note that the maximum point moves by about 20 degree in Gouy phase as the interferometer goes from the cold to the hottest possible state. Not much of a variation in demodulation angle due to heating is observed in that range of Gouy phase.

Fig.12 shows extreme cases of differential heating when either ITMX or ITMY is heated. There is very minor difference in heating of ITMX or ITMY and that difference is suppressed in this plot. Again, not much of variation in demodulation angle is observed in the Gouy phase range of interest: 90 to 120 degrees.

6 Concluding Remarks

The heating affects WFS signals in several ways. The best mode-matched condition for LIGO is achieved for the saturated hottest state with the designed parameter. First of all, the signal amplitudes get reduced if the IFO is in a cooler state due to the generation of higher order modes for sidebands and the consequent reduction in its TEM00 content. However, the mea-

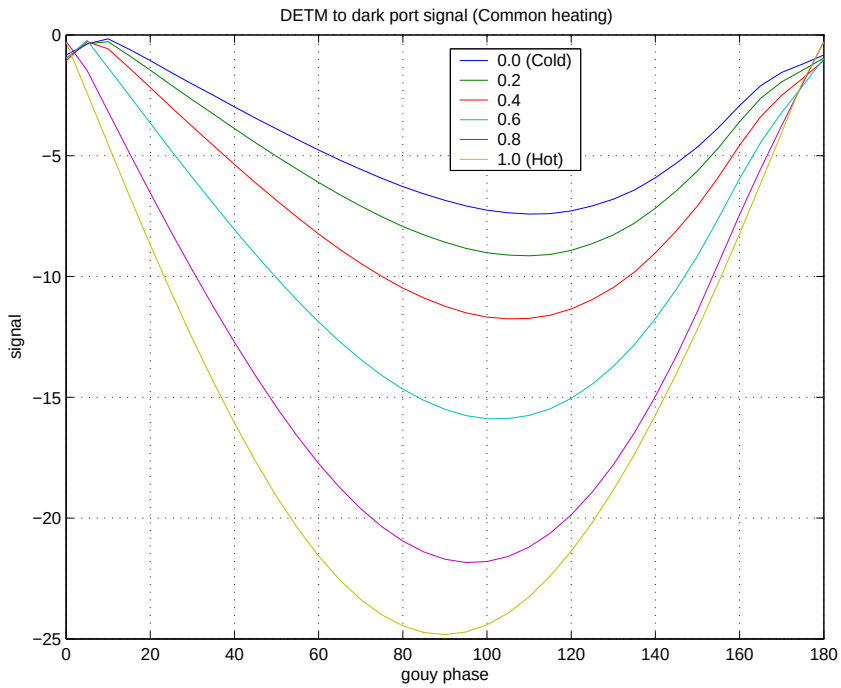

Figure 11: WFS1 signal for DETM dof under various states of Common heating as function of Gouy phase from dark port.

sured signals may also get affected by inappropriate setting of the gouy phase telescope which is also a function of heating. The best values for Gouy phases for the detected signals may change due to the variation in amplitudes of sidebands, which originates from varying level of modal mismatch. For WFS 3 and 4 at the reflected port this is particularly crucial where good choice of telescope setting is important for separating contributions of two different degrees of freedom. The measurements at H1 conform with these observation. In WFS 2, the choice of the Gouy phase location is less ambiguous - around 145 degree. However, changes in demodulation angle as a function of heating have been observed there. These changes seem to originate mainly from both the common and differential heating of DITM dof. Simulation shows that differential heating affects amplitudes and phases of upper and lower sidebands differently which finally contributes to such changes in demodulation angles. Currently the rotation of demodulation angle observed in H1 seem to be quantitativelty larger than what could be explained from a combination of common and differential heating. More measurements and analysis would be necessary to make these numbers agree quantitatively.

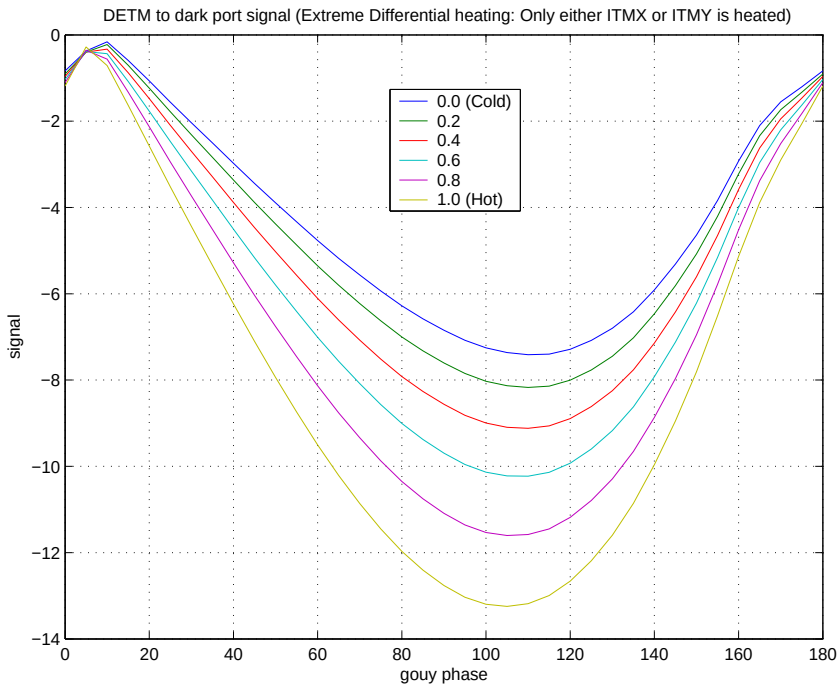

Figure 12: WFS1 signal for DETM dof under various states of an example of extreme differential heating as function of Gouy phase from dark port.

References

[1] B. Kells, J. Camp, “Absorption in the Core Optics and LIGO sensitivity”, LIGO document no. T970097-01 (LIGO Laboratory, Caltech, Pasadena, USA, 1998).

[2] Bochner, B., “Modeling the performance of Interferometric Gravitational-wave detectors with realistically imperfect optics”, Ph.D theses (MIT, 1998), LIGO Doc. P980004-00R.

[3] P. Fritschel, N. Mavalvala, D. Shoemaker, D. Sigg, M. Zucker, G. Gonzalez, “Alignment of an interferometric gravitational wave detector”, Applied Optics, **37**, 6734-6747 (1998).

[4] P. Hello, J.Y. Vinet, J. Phys (Paris), **51**, 2243 (1990); W. Winkler, K. Danzmann, A. Rüdiger, R. Schilling, “Heating by optical-absorption and the performance of interferometric gravitational-wave detectors”, Phys. Rev. A, **44**, 7022-7036 (1991).

[5] D. Sigg, N. Mavalvala, “Principles of calculating the dynamical response of misaligned complex resonant optical interferometers”, JOSA, A17, 1642-1649 (2000)

[6] B. Bhawal, M. Evans, M. Rakhmanov, V. Sannibale, H. Yamamoto, Proceedings of the XXXVIIIth Rencontres de Moriond workshop on “Gravitational Waves and Experimental Gravity” Les Arcs, France, March 22-29, 2003, edited by J. Dumarchez and J. Tran Thanh Van, pp. 131-138 (The Gioi Publishers, Vietnam, 2004)

[7] B. Bhawal, M. Evans, H. Yamamoto, “The wave-front signals from E2E’s 6-optics LIGO system”, LIGO document no. T030016 (2003).

[8] L. Matone, Hanford detector elog, Feb 6, Feb 24, 2004.

[9] L. Matone, Hanford detector elog, Sep 5-6,26, 2003